

## **ANALYTICAL TREATMENT OF SCHLIEREN METHOD FOR PRECISE QUANTITATIVE CHARACTERISATION OF FLUID DYNAMICS**

**V.I.Vlad and N. Ionescu-Pallas**

Institute of Atomic Physics, NILPRP-Romanian Center of Excellence in Photonics and The  
Romanian Academy-CASP, Bucharest, P.O.Box MG-36, ROMANIA  
E-mail: vlad@ifin.nipne.ro

**Abstract.** A quantitative analysis of the Schlieren images, characterized by high accuracy (comparable to the interferometric methods), is presented. We find new analytical formulae relating the intensity distribution in the Schlieren image to the refraction index gradient distribution in the fields of transparent fluids, in the special cases of the flows around planar (thin) structures and axi-symmetric ones. The digital processing of the Schlieren image is suitable corrected and calibrated and by using our formulae, leads to precise measurement of the refraction index gradient distribution in a supersonic flow. Then, utilising the Gladstone-Dale relation, we determine the distributions of mass density and of pressure in the flow, which are coinciding with the results of theoretical modelling of the flow in the limits of 5%. Moreover, we give here a generalization of our analytical results to the cases of fluid flows without symmetry, which allows the tomographic visualisation of these flows.

Key words: Schlieren, fluid flow, fluid tomography, supersonic flows

### **1. INTRODUCTION**

The complex problems of the mass and heat transfer in the fluid dynamics can be seriously simplified by the visualisation of the corresponding processes. An image of the flow could bring important information for the quantitative description of the fluid dynamics and for the some convenient analytical solutions. The flow visualisation can also focus other quantitative measurements to the domains of interest.

A widespread optical, non-invasive method for the visualisation of the phase inhomogeneities in the transparent media and of their spatio-temporal evolution is the Schlieren method [1-4]. The Schlieren method is frequently used in the qualitative analysis of the refraction index gradient in fluid flows. In transparent fluid flows, the refraction index gradient distribution can be correlated to the corresponding distributions of density, temperature and pressure.

Previous works tried to give a quantitative interpretation of the Schlieren images with precise analytical solutions of the corresponding inverse problem (obtaining the refraction index gradient distribution from the intensity distribution in the Schlieren image) [5-22]. However, a general analytical treatment and experimental tests of its accuracy are still matters of research.

In the present work, we give a quantitative analysis of the Schlieren images, characterized by high accuracy (comparable to the interferometric methods), in a more simple and less expensive visualisation system. We present new analytical formulae relating the intensity distribution in the Schlieren image to the refraction index gradient distribution in the fields of

transparent fluids, in the special cases of the flows around planar (thin) structures and axisymmetric ones. The digital processing of the Schlieren image was suitably corrected and calibrated and by using our formulae, led to the precise measurement of refraction index gradient distribution in a supersonic flow. Then, utilising the Gladstone-Dale relation, we have determined the distribution of mass density in that flow, which is coinciding, with the results of the theoretical model of the flow in the limits of 5% [5, 6].

Moreover, we have generalized our analytical results to the fluid flows without symmetry, by using a Radon-type transform, which allows the tomographic visualisation of these flows.

## 2. A QUANTITATIVE SCHLIEREN METHOD

A typical Schlieren system with lenses and a “knife-edge” filter oriented perpendicularly to the  $x$ -axis is shown in Fig.1. If the complex amplitude of the input optical field ( $(x'O'y')$ ), at the entrance window of the transparent fluid (IN), is described by the 2D complex function:  $f_{ob}(x', y') = \sqrt{I_0} e^{i\varphi(x', y')}$ , the distribution of the optical field in the output plane (OUT,  $(xOy)$ ) is:

$$g(-x, -y) = \int_{-\infty}^{+\infty} \int_{-\infty}^{+\infty} h\left(x - \frac{f_2}{f_1} x', y - \frac{f_2}{f_1} y'\right) f_{ob}(x', y') dx' dy' . \quad (1)$$

where  $f_1$  and  $f_2$  are the focal distances of the Fourier lenses.

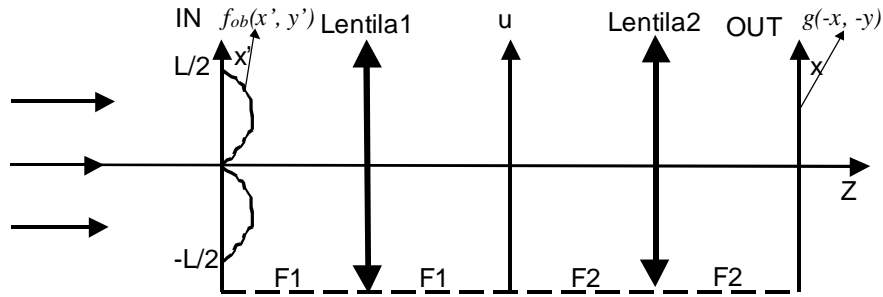


Fig.1. Schlieren system with lenses.

Considering in (1) the explicit expression for the impulse response of the linear amplitude filter:

$$h\left(x - \frac{f_2}{f_1} x', y - \frac{f_2}{f_1} y'\right) = \int_{-\infty}^{+\infty} \int_{-\infty}^{+\infty} \frac{H(u, v)}{\lambda^2 f_1 f_2} \exp\left\{ \frac{2\pi i}{\lambda f_2} \left[ \left( x - \frac{f_2}{f_1} x' \right) u + \left( y - \frac{f_2}{f_1} y' \right) v \right] \right\} dudv, \quad (2)$$

$$H(u, v) = \begin{cases} 0, & -\infty < u < \infty \\ \frac{1}{2} + \frac{u}{L}, & (-L/2) < u < (L/2) \\ 1, & (L/2) < u < \infty \end{cases} ,$$

with  $L$ , the Schlieren system aperture dimension (equal to the light beam diameter in the input plane), the light intensity in the output plane can be found as [5, 6]:

$$I(x, y) = |g(-x, -y)|^2 = \frac{1}{4} I_0 \left( \frac{f_1}{f_2} \right)^2 \left\{ 1 + \frac{\lambda f_2}{\pi L} \cdot \frac{\partial \varphi[(f_1/f_2)x, (f_1/f_2)y]}{\partial x} \right\}^2, \quad (3)$$

in which  $I_0$  is the uniform light intensity in front of the input plane (and can be measured also in the output plane, in an unperturbed flow zone) and  $\lambda$  is the light wavelength. We introduce the notations:

$$I_\infty = \frac{1}{4} I_0 \left( \frac{f_1}{f_2} \right)^2; \quad n_s = n \left( \frac{f_1}{f_2} x, \frac{f_1}{f_2} y, \frac{f_1}{f_2} z \right); \quad \varphi(x, y) = \frac{2\pi}{\lambda} \int_{-\infty}^{\infty} [n_s(x, y, z) - n_\infty] dz \quad (4)$$

and  $n_\infty$  for the fluid refraction index (in a stationary/unperturbed zone) and Eq.(3) can be cast in the form:

$$1 - \sqrt{\frac{I(x', y)}{I_\infty}} = \frac{2f_1}{L} \frac{\partial}{\partial x} \int_{-\infty}^{\infty} [n_\infty - n_s(x, y, z)] dz. \quad (5)$$

In geometrical terms, up to the constant  $(2f_1/L)$ , the right hand side of Eq.(5) can be identified to the tangent of the vertical deviation angle of the light rays due to the perturbing object from the input plane. Thus, we can denote:

$$\frac{L}{2f_1} \left[ 1 - \sqrt{\frac{I(x', y)}{I_\infty}} \right] = \tan \varepsilon_x; \quad (\text{on Ox}) \quad \tan \varepsilon_x \approx \varepsilon_x.$$

By integrating in Eq.(5) with respect to  $x$ , we obtain:

$$\int_x^\infty \left[ 1 - \sqrt{\frac{I(x', y)}{I_\infty}} \right] dx' = \frac{2f_1}{L} \int_{-\infty}^{\infty} [n_s(x, y, z) - n_\infty] dz. \quad (6)$$

Thus, the problem of Schlieren image analysis, namely the determination of the refraction index distribution in the input plane from the output light intensity distribution (Schlieren image), can be solved using Eq. (6). For its effective solving, we shall analyse, firstly, two particular cases, which are important in applications.

### Case 1. Thin (planar, 1D) object

In this case,  $n_s(x, y, z)$  does not depend on the coordinate  $z$  and the inversion in Eq.(6) is straightforward. The distribution of refractive index in the input plane can be obtained as [5]:

$$n \left( \frac{f_1}{f_2} x, \frac{f_1}{f_2} y \right) - n_\infty = \frac{L}{2f_1} \int_x^\infty \left( 1 - \sqrt{\frac{I(x', y)}{I_\infty}} \right) \frac{dx'}{d}, \quad (7)$$

where  $d$  is the constant thickness of the object in transversal direction, Oz.

### Case 2. Axial-symmetric object (around Oy-axis)

A section through the object with the plane  $y = \text{constant}$  is presented in Fig.2.



Thus, the first inverse problem in the Schlieren method is solved and we can calculate exactly the refraction index distribution from the intensity distribution recorded in the Schlieren image, given  $f_1$ ,  $f_2$ ,  $n_\infty$ ,  $L$  and  $I_0$ .

For the cases 1 and 2, the optical object is formally divided in planes, which are parallel to the plane  $xOz$ . At the height of such a plane,  $y_k$ , we can successively apply the previous formulae and we can reconstruct the refraction index spatial distribution from the set of two-dimensional distributions in the planes  $y_k$ .

### Case 3. Non-symmetrical objects

We consider that the phase object is immersed in a matching fluid, such as its phase is small:

$$\frac{n(x, y) - n_L}{n_L} \ll 1. \quad (12)$$

The above described method for axial-symmetric objects could be generalised for the visualisation and the measurement of the non-symmetric objects with refraction index distribution (RID), which satisfy the condition (12). The experimental set-up is similar to that of Fig.1, but the Schlieren intensity distribution (SID) must be recorded in different angular positions of the object,  $\theta$ , which is rotated around the origin of the coordinate system. In the general case, when  $n = n(x, y, z)$ , RID can be determined in different sections considering only the ray trajectory projections on the plane  $xOy$ .

Let us consider a coordinate system,  $x'Oy'$ , which is rotated by the angle  $\theta$  with respect to the object coordinate system,  $xOy$ , in which:

$$x = x' \cos \theta - y' \sin \theta \quad (13)$$

$$y = x' \sin \theta + y' \cos \theta$$

Due to the small variations of the refractive index, the changes of the light ray directions in the phase object are as well small. Thus, the input ray which is incident at the height  $x' = p$  and has the slope  $dx'/dy' = 0$  will leave the object with the slope:

$$\varepsilon_x(p, \theta) \approx \left( \frac{dx'}{dy'} \right)_s = \frac{1}{n_s} \int_{-\infty}^{\infty} \frac{\partial n(x, y)}{\partial x'} dy' = \frac{1}{n_s} \int_{-\infty}^{\infty} \frac{\partial n}{\partial p} (p \cos \theta - y' \sin \theta, p \sin \theta + y' \cos \theta) dy' = \frac{1}{n_s} \frac{\partial}{\partial p} N(p, \theta) \quad (14)$$

where we have denoted:

$$N(p, \theta) = \int_{-\infty}^{\infty} [n(p \cos \theta - y' \sin \theta, p \sin \theta + y' \cos \theta) - n_s] dy' \quad (15)$$

$$= \int_{-\infty}^{\infty} \int_{-\infty}^{\infty} [n(p \cos \theta - y' \sin \theta, p \sin \theta + y' \cos \theta) - n_s] \delta(p - x') dx' dy'.$$

In Eq. (15),  $\delta$  is delta distribution. Formally, in Eqs. (14-15) the integration limits are chosen at  $\pm\infty$ , in spite of the fact that RID and its slope vanish outside the object.

If we write RID in cylindrical coordinates,  $n(r, \varphi) = n(x, y)$ , Eq. (15) becomes:

$$N(p, \theta) = \int_{-\infty}^{\infty} \int_{-\infty}^{\infty} [n(r, \varphi) - n_s] \delta[p - r \sin(\varphi - \theta)] dr d\varphi. \quad (16)$$

Equation (16) is the Radon transformation of the function  $n - n_s$ . Assuming that the planar section of the object is contained inside of a circle with the radius  $R$  and with the center in the origin of the coordinate system, Eq.(16) could be inverted as [4, 13 ]:

$$n(r, \varphi) - n_L = \frac{1}{2\pi^2} \int_{-\pi/2}^{\pi/2} d\theta \int_{-R}^R \frac{(\partial N / \partial p) dp}{r \sin(\varphi - \theta) - p} \tag{17}$$

Moreover, we can write RID as an integral transformation of the light ray deflection angle:

$$\frac{n(r, \varphi) - n_L}{n_L} = \frac{1}{2\pi^2} \int_{-\pi/2}^{\pi/2} d\theta \int_{-R}^R \frac{\varepsilon_x(p, \theta) dp}{r \sin(\varphi - \theta) - p} . \tag{18}$$

Due to the integrand singularity for  $p = r \sin(\varphi - \theta)$ , the second integral in Eq.(18) must be interpreted in the sense of the Cauchy principal value.

If the light ray deflection angle is taken as in Eq.(14 ), (18) becomes:

$$n\left(\frac{f_1}{f_2} r, \varphi, \frac{f_1}{f_2} z\right) = \frac{1}{(2\pi)^2} \frac{L}{f_1} \cdot \int_{-\frac{\pi}{2}}^{+\frac{\pi}{2}} d\theta \cdot \int_{-R}^{+R} \frac{\sqrt{\frac{I(p, \theta; z)}{I_\infty}} - 1}{r \cdot \sin(\varphi - \theta) - |p|} dp , \tag{19}$$

which is a generalisation of Abel-type equation from (11) by a Radon-type integral transformation. When  $I$  is independent on  $\theta$  , we have:

$$K(p, r) \equiv \int_{-\frac{\pi}{2}}^{+\frac{\pi}{2}} \frac{d\theta}{r \cdot \sin(\varphi - \theta) - |p|} = \begin{cases} 0, & \text{for } p^2 < r^2 \\ -\frac{\pi}{\sqrt{p^2 - r^2}}, & \text{for } p^2 > r^2 \end{cases} \tag{20a}$$

so that:

$$\int_{-\frac{\pi}{2}}^{+\frac{\pi}{2}} d\theta \int_{-R}^{+R} \frac{\left(\frac{I}{I_\infty}\right)^{1/2} - 1}{r \sin(\varphi - \theta) - |p|} dp = -\pi \left\{ \int_{-R}^{-r} \frac{\left(\sqrt{\frac{I}{I_\infty}} - 1\right)}{\sqrt{p^2 - r^2}} dp + \int_r^R \frac{\left(\sqrt{\frac{I}{I_\infty}} - 1\right)}{\sqrt{p^2 - r^2}} dp \right\} = 2\pi \int_r^R \frac{\left(1 - \sqrt{\frac{I}{I_\infty}}\right)}{\sqrt{p^2 - r^2}} dp \tag{20,b}$$

and the result from Eq.(11) is again obtained.

In (19), we can denote:  $I(p) \equiv I(p, \theta, z) / I_\infty$  and after a simple change of the integration domain of the variable  $p$ , we can obtain:

$$n\left(\frac{f_1}{f_2} r, \varphi, \frac{f_1}{f_2} y\right) = \frac{1}{(2\pi)^2} \frac{L}{f_1} \cdot \int_{-\frac{\pi}{2}}^{+\frac{\pi}{2}} d\theta \cdot \int_0^{+R} \frac{\sqrt{I(-p)} + \sqrt{I(+p)} - 2}{r \cdot \sin(\varphi - \theta) - p} dp \tag{21}$$

Integrating by parts in the second integral from Eq.(21), one gets the final formula:

$$n\left(\frac{f_1}{f_2} r, \varphi, \frac{f_1}{f_2} z\right) = \frac{1}{(2\pi)^2} \frac{L}{f_1} \cdot \int_{-\frac{\pi}{2}}^{+\frac{\pi}{2}} d\theta \cdot \int_0^{+R} \left( \ln \left| \sin(\varphi - \theta) - \frac{p}{r} \right| \right) \frac{\partial}{\partial p} \left[ \sqrt{I(-p)} + \sqrt{I(+p)} \right] dp . \tag{22}$$

Eq.(22) represents the general equation of the Schlieren tomography, which allows the RID reconstruction for non-symmetrical objects from intensity measurements in Schlieren images.

### 3. CALCULATION OF THE MASS DENSITY FROM RID

A second inverse problem in the quantitative Schlieren method is the determination of the mass density using the measured RID. This problem is dependent on the fluid type.

In the air flows, used in aerodynamics, *the density distribution* can be calculated from RID by using Gladstone-Dale relation [1]:

$$n - 1 = 2,94 \times 10^{-4} \frac{\rho}{\rho_0}, \quad (23)$$

where  $\rho_0$  is undisturbed (stationary) air density.

Finally, the density and the pressure are related by well-known equations:

$$\frac{\rho}{\rho_\infty} = \frac{(\gamma - 1)p_\infty + (\gamma + 1)p}{(\gamma - 1)p + (\gamma + 1)p_\infty} \quad (\text{Rankine-Hugoniot eq., in the region of the shock waves})$$

$$\frac{\rho}{\rho_\infty} = \left( \frac{p}{p_\infty} \right)^{\frac{1}{\gamma}} \quad (\text{adiabatic eq., outside of region with the shock waves, } \gamma = 7/5),$$

and *the pressure distribution* can be calculated everywhere in the air flow.

For liquids [1, 20], the density distribution can be calculated from the refractive index by Lorenz-Lorentz equation:

$$n^2 - 1 / (n^2 + 2)\rho = A, \quad (24)$$

where A is the molecular refractivity. For water, it was measured:  $A = 0.206$  (at  $\lambda = \lambda_D$ , natrium line). This relation is experimentally proved from the vapour state to 4°C with precision (2-3)% and for pressure increase of 1800 atm. The water density changes very little with the pressure and temperature. For example: at 0°C and 1.0 atm,  $\rho = 1.000 \cdot 10^3 \text{ Kg/m}^3$ ; at 100°C and 1.0 atm,  $\rho = 0.958 \cdot 10^3 \text{ Kg/m}^3$ ; at 0°C and 50 atm,  $\rho = 1.002 \cdot 10^3 \text{ Kg/m}^3$ . If we consider the incompressible fluid, the refractive index will exhibit no change with the pressure variations.

Though, the refraction index changes with the temperature are not negligible [15]. For water, at 300°K, the following dependencies were found:

$$-dn/dT [\text{K}^{-1}] = 1.00 \cdot 10^{-4} \quad (546\text{nm})$$

$$= 0.985 \cdot 10^{-4} \quad (633\text{nm})$$

$$\text{and} \quad n - 1.337253 = -(2.8767 T + 0.14825 T^2) \cdot 10^{-5} \quad (546\text{nm})$$

$$n - 1.3331733 = -(1.936 T + 0.1699 T^2) \cdot 10^{-5} \quad (633\text{nm})$$

### 4. PRECISE NUMERICAL ALGORITHM FOR THE QUANTITATIVE SCHLIEREN METHOD, IN THE CASE OF AXI-SYMMETRICAL OBJECTS

For axi-symmetrical objects, we can introduce the notations:  $r' = \tau r_\infty$  and  $r = \zeta r_\infty$  and the variable change:

$$\eta = \frac{\ln\left[\left(\tau + \sqrt{\tau^2 - \zeta^2}\right)/\zeta\right]}{\ln\left[\left(1 + \sqrt{1 - \zeta^2}\right)/\zeta\right]}, \quad (25)$$

which leads to the new form of Ec. (11):

$$n\left(\frac{f_1}{f_2}\zeta, r_\infty, \frac{f_1}{f_2}y\right) - n_\infty = \frac{S(\zeta)^{+1}}{2\pi} \int_{-1}^{+1} f(\eta) d\eta, \quad (26)$$

with:

$$S(\zeta) = \ln\left[\left(1 + \sqrt{1 - \zeta^2}\right)/\zeta\right] \quad \text{and} \quad f(\eta) = 1 - \sqrt{\frac{I(\tau_\infty, z)}{I_\infty}}. \quad (27)$$

The integral in Eq. (26) can be calculated by sums using the Tschebyshev polynomial method:

$$\frac{1}{2} \int_{-1}^{+1} f(\eta) d\eta = \frac{1}{2N+1} \left\{ f(0) + \sum_{k=1}^{k=N} \left[ f\left(-\frac{k}{N+0.5}\right) + f\left(+\frac{k}{N+0.5}\right) \right] \right\} \quad (28)$$

where N is the number of equally spaced experimental points.

Finally, the distribution of refractive index (RID) can be written as:

$$n\left(\frac{f_1}{f_2}\zeta, r_\infty, \frac{f_1}{f_2}z\right) - n_\infty = \frac{1}{\pi} \ln\left[\left(1 + \sqrt{1 - \zeta^2}\right)/\zeta\right] \cdot \frac{1}{2N+1} \left\{ \left[ 1 - \sqrt{I\left(\frac{f_1}{f_2}\zeta, r_\infty, \frac{f_1}{f_2}z\right)/I_\infty} \right] + 2 \sum_{k=1}^{k=N} \left[ 1 - \sqrt{I\left(\frac{f_1}{f_2}\zeta, r_\infty \tau_k, \frac{f_1}{f_2}z\right)/I_\infty} \right] \right\} \quad (29)$$

$$\text{with: } \tau_k = \frac{1}{2} \zeta^{\frac{N-k+0.5}{N+0.5}} \left\{ \left(1 + \sqrt{1 - \zeta^2}\right)^{\frac{k}{N+0.5}} + \left(1 - \sqrt{1 - \zeta^2}\right)^{\frac{k}{N+0.5}} \right\}. \quad (30)$$

## 5. EXPERIMENTAL RESULTS. TESTING THE ANALYTICAL FORMULAE FOR THE SCHLIEREN METHOD

Our experiments were done with a standard Schlieren system (with continuous and pulsed quasi-monochromatic illumination) at a supersonic aerodynamic flow tunnel. The Schlieren images were recorded on a standard photographic film (35 mm, 100-200ASA large dynamics, flexibility in exposure time and high resolution)

The recorded images were read-out by a TV camera and digitised in an array of 256x256 pixels with 256 grey levels. The TV camera constant,  $\gamma_c$ , was determined using a calibrated step density mask in each Schlieren image, in a region corresponding to the free flow). The film constant,  $\gamma_f$ , was determined by using a step density mask (an exposed film with known density steps recorded at known uniform illuminations and different exposure times), which was fixed on the aerodynamic tunnel window.

The Schlieren image was calibrated in a fixed point with the data given by a pressure sensor:

$$n(r_s, \zeta_s) - n(r_{sw}, \zeta_s) = \mathbf{F}$$

where the index "s" is associated to the sensor location and the index "sw" to the coordinates of a point situated immediately under the shock wave, for which the ratio  $\rho_{sw}/\rho_\infty$  is given, with ago approximation, by the Mach number only. In our case,  $\rho_{sw}/\rho_\infty = 1.43$ .

Denoting by:

$$\rho(r_s, \zeta_s) = \rho_s ; \rho(r_{sw}, \zeta_s) = \rho_{sw}$$

$$n(r_s, \zeta_s) = n_s ; n(r_{sw}, \zeta_s) = n_{sw}$$

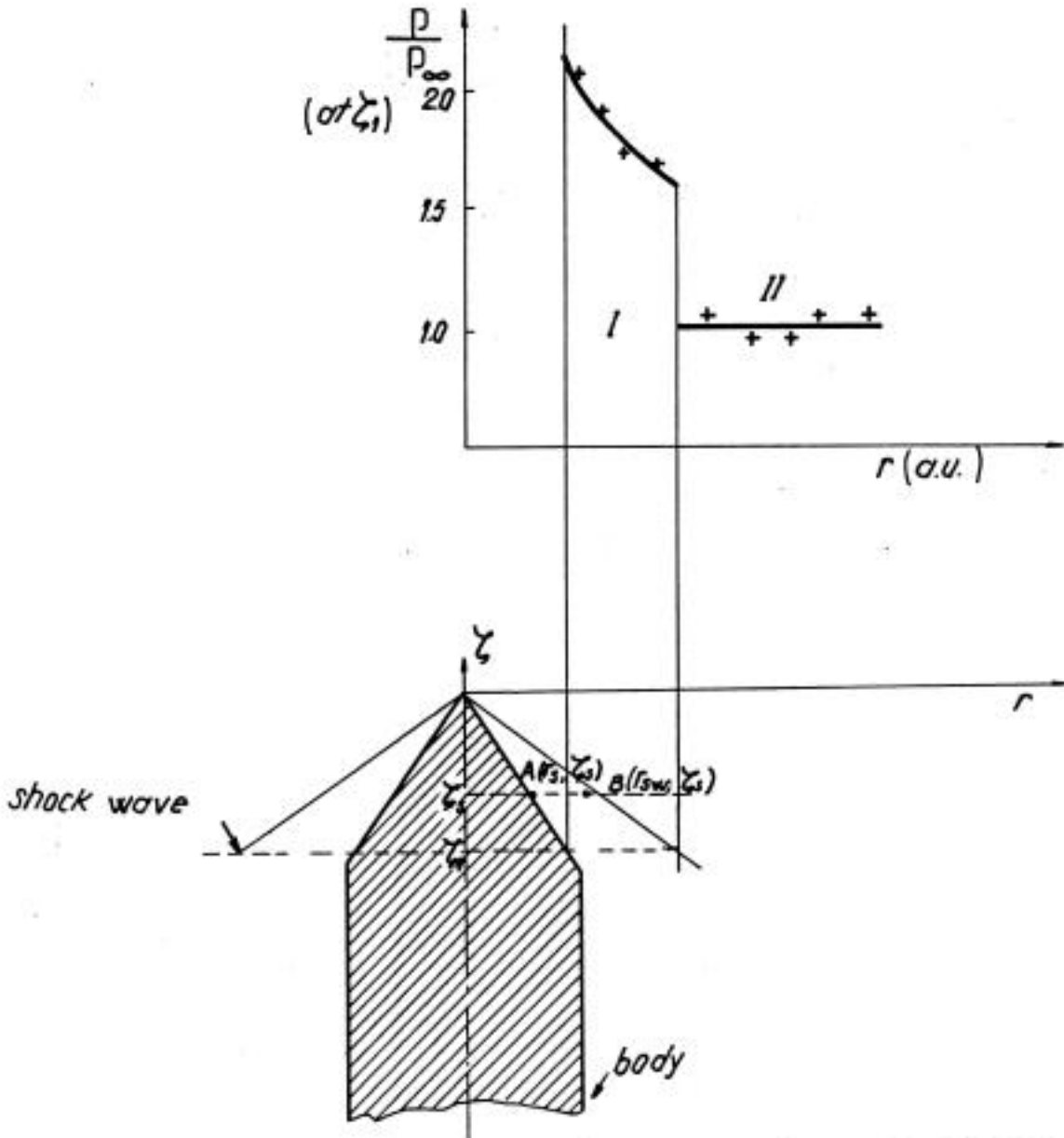


Fig.3. Quantitative results obtained using Eq. (29) for processing Schlieren images of a supersonic flow (crosses) and the theoretical predictions of the aerodynamic modelling (solid lines)

for an arbitrary point situated on a line between the shock-wave and the model, perpendicular to the model axis (Fig.3), the Gladstone-Dale relation leads to the determination of the air density in the region of interest of the flow as:

$$\frac{\rho}{\rho_{sw}} = 1 + \left( \frac{\rho_s}{\rho_{sw}} - 1 \right) \frac{\mathbf{F}(r, \zeta_1)}{\mathbf{F}(r_s, \zeta_s)} \quad (31)$$

Adiabatic equation gives the results:

**conic surface:**  $(p / p_\infty)_{\text{exp}} = 2.10 \pm 0.03$  ; theoretical prediction and sensor:  $p / p_\infty = 2.11$ ;

**cylindrical surface:**  $(p / p_\infty)_{\text{exp}} = 0.81 \pm 0.5$ ; - " -  $p / p_\infty = 0.78$ .

The quantitative Schlieren method developed by us offers also the possibility to measure the pressure in an arbitrary point of the flow, for example, a constant pressure on a conic surface co-axial with the shock wave surface and with the same apex:

$$tg\theta_1 = 0.8; \left( \frac{\rho}{\rho_\infty} \right)_{\text{exp}} = 1.92 \pm 0.04$$

$$tg\theta_2 = 1.05; \left( \frac{\rho}{\rho_\infty} \right)_{\text{exp}} = (1.75 \pm 0.02)$$

where  $\theta$  is the half-angle of the isobar-cone.

Moreover, the experimental dependence of the ratio  $p / p_\infty$  can be determined in function of the radial distance on the cone surface for  $\zeta_1 = 0.837 h$ , ( $h$  is the cone height) (Fig.3). Both regions under the shock wave (I) and over the free flow (II) are clearly and precisely characterised. The discontinuity of the air pressure distribution at the passage through the shock wave is clearly illustrated in the experimental data.

## 6. CONCLUSIONS

In this paper, we have obtained new analytical results for the precise quantitative interpretation of the Schlieren images:

- for planar phase objects (e.g. wings);
- for phase objects with axial symmetry (e.g. cylindrical and conical parts), by Abel-type tomographic inversion;
- for non-symmetrical phase objects, by Radon-type tomographic inversion.

In the case of axi-symmetrical phase objects, we have elaborated a precise numerical algorithm also, which simplifies the software for the experimental data processing. The analytical results were verified in experiments with supersonic tests of cylindrical and conical models. Processing of the experimental data with our algorithm and with careful corrections and calibrations leads to a good agreement between the experiments and the theoretical predictions of the aerodynamic modelling.

## REFERENCES

1. W. Merzkirch, "Flow Visualisation", Academic Press, 1987
2. H. Lipson, "Optical Transforms", Academic Press, 1972.

3. V.I.Vlad, R.Zaciu, J.Maurer, N. Miron si D.Sporea, Prelucrarea optica a informatiei, Editura Academiei Romane, 1974
4. W. Hauf, U. Grigull, 'Optical Methods in Heat Transfer', in J. P. Hartnett, T. F. Irvine, Jr., Eds., *Advances in Heat Transfer*, Academic Press, New York, London, 1970, pp. 133 – 366.
5. V. I. Vlad, N. Ionescu-Pallas, I. Apostol, "Accurate refractive index measurements using computerised Schlieren and focusing methods", Proc. SPIE, **1319**, 649 –654(1990) and *Rev. Roum. Phys.*, **36**, 915 – 922(1991)
6. V. I. Vlad, N. Ionescu-Pallas, I. Apostol, 'Quantitative Schlieren method using digital image processing for supersonic flow characterization', Proc. SPIE, **1771**, 1771 – 1774(1992)
7. Greenberg, P.S., Klimek, R.B., Buchele, D.R., Quantitative Rainbow Schlieren Deflectometry, *Applied Optics*, **34** (19), 3810-3822(1995).
8. Weinstein, L., An Improved Large-Field Focusing Schlieren System, AIAA Paper 91-0567., 29th Aerospace Sciences Meeting, Reno, January 7-10, 1991.
9. Doggett, G, and Chokani, N.: A Large-Field Laser Holographic Focusing Schlieren System, AIAA Paper 92-3936, 17th Aerospace Ground Testing Conference, Nashville, July 6-8 1992.
10. Cook, S, and Chokani, N.: Quantitative Results From The Focusing Schlieren Technique, AIAA Paper 93-0630, 31st Aerospace Sciences Meeting, Reno, January 11 -14, 1993.
11. Alvi, F.,and Settles, G.: A Sharp-Focusing Schlieren Optical Deflectometer. AIAA Paper, 93-0629, 31st Aerospace Sciences Meeting , January 11-14,1993.
12. Weinstein, L.: A Large-Field High-Brightness Focusing Schlieren System. *AIAA Journal*, **31**(7), 1250-1255(1993)
13. V.I.Vlad, N. Ionescu-Pallas and Fl. Bociort, New treatment of the focusing method and tomography of the refractive index distribution inside the inhomogeneous optical components, *Optical Eng.* **35**(5), 1305(1996)
14. Carpenter P.W, Green P.N, The aeroacoustics and aerodynamics of high-speed Coanda devices, Part 1: Conventional arrangement of exit nozzle and surface, *Journal of Sound and Vibration*, **208**(5), 777-801(1997)
15. Agrawal A.K., Butuk N.K., Gollahalli S.R, Griffin D., Three-dimensional rainbow schlieren tomography of a temperature field in gas flows, *Appl. Optics*,**37**(3), 479-485(1998).
16. Brysev A.P, Krutyanskii L.M, Preobrazhenskii V.L, Wave phase conjugation of ultrasonic beams, *Uspehi Fiz. Nauk*, **168**(8), 877-890 (1998)
17. Bystrov S.A, Honma H., Ivanov V.I, Koreeda J., Maeno K, Shugaev F.V, Yanagisawa\_H, Density reconstruction from laser schlieren signal in shock tube experiments, *Shock Waves*, **8** (3), 183-189(1998)
18. Shenoy A.K, Agrawal A.K, Gollahalli S.R, Quantitative evaluation of flow computations by rainbow Schlieren deflectometry, *AIAA Journal*, **36**(11), 1953-1960(1998)
19. AlAmmar K, Agrawal A.K, Gollahalli S.R, Griffin D, Application of rainbow schlieren deflectometry for concentration measurements in an axisymmetric helium jet, *Experiments in Fluids*, **25**(2), 89-95(1998)
20. Noack J, Vogel A, Single-shot spatially resolved characterization of laser-induced shock waves in water, *Appl. Optics*, **37**(19), 4092-4099(1998)
21. Tanda G, Devia F, Application of a schlieren technique to heat transfer measurements, *Experiments in Fluids*, **24**(4), 285-290(1998)

22. Iwase O, Suss W, Hoffmann D.H.H, Roth M, Stockl C, Geissel M, Seelig W, Bock R, Laser-produced plasma diagnostics by a combination of Schlieren method and Mach-Zehnder interferometry, *Physica Scripta*, **58**(6), 634-635(1998)
23. Greenberg P.S, Weiland K.J, VanderWal R.L, Microgravity combustion diagnostics: the path to the International Space Station, *Measurement Science & Technology*, **10**(10), 831-835(1999)
24. Dubois F, Joannes L, Dupont O, Dewandel JL, Legros JC , An integrated optical set-up for fluid-physics experiments under microgravity conditions, *Measurement Science & Technology*, **10**(10), 934- 945(1999)
25. Kimmel R.L, Poggie J, Schwoerke S.N, Laminar-turbulent transition in a Mach 8 elliptic cone flow, *AIAA Journal*, **37**(9), 1080-1087(1999)
26. Zakharin B, Stricker J, Toker G, Laser-induced spark Schlieren imaging, *AIAA Journal*, **37**(9), 1133-1135(1999)
27. DeWispelaere E, Malka V, Huller S, Amiranoff F, Baton S, Bonadio R, Casanova M, Dorchie F, Haroutunian R, Modena A, Formation of plasma channels in the interaction of a nanosecond laser pulse at moderate intensities with helium gas jets, *Physical Review E*, **59**(6), 7110-7120(1999)
28. Agrawal A.K, Albers B.W, Griffin D.W, Abel inversion of deflectometric measurements in dynamic flows, *Applied Optics*, **38**(15), 3394-3398(1999)
29. Kochetov I.V, Mazalov D.A, Pal A.F, Filippov A.V, Study of spherical shock waves in a non-self-maintained discharge by the laser schlieren technique, *Plasma Physics Reports*, **25**(5), 375-386(1999)
30. Muller R, Marquard J, The Hilbert transform and its generalization in optics and image processing, *Optik*, **110**(2), 99-109(1999)
31. Bibbo L, Giovambatista N, Gomez P, Olivieri M, Tibaldi C, Bernal L, Pouzo J, Bilbao L, Optical measurements in an exploding wire experiment, *Astrophysics and Space Science*, **256**, 467- 472(1998)
32. Woodcraft A.L, Lucas P.G.J, Matley R.G, Wong W.Y.T, Visualisation of convective flow patterns in liquid helium, *J. Low Temperature Physics*, **114**, 109-134(1999)
33. A.Petris, D.Popa, A.Jianu, C.Popa and V.I. Vlad, Optoelectronic Visualization and Study of Heat Transfer from Metal Wires to Water by a Compact Schlieren System, *Proc. SPIE*, **4068**, 491-6(2000)
34. A.Petris, C.Popa, D.Popa, V.I.Vlad, Visualization and Study of the Heat Diffusion in Glass by a Compact Schlieren System, *Proc. SPIE, ROMOPTO 2000*
35. M.Kurzeluk, A.Guzun, A.Petris, V.I.Vlad, Study of phenol adsorption using real-time holographic interferograms in photorefractive crystals, *Proc. SPIE, ROMOPTO 2000*

